

High Velocity Outflows in Narrow Absorption Line Quasars

G. Chartas, J. Charlton, M. Eracleous, M. Giustini, P. Rodriguez Hidalgo

*Department of Astronomy & Astrophysics, Pennsylvania State University, University
Park, PA 16802, chartas@astro.psu.edu*

R. Ganguly

*Department of Computer Science, Engineering, & Physics, University of Michigan-Flint,
Flint, MI 48502*

F. Hamann

*Department of Astronomy, University of Florida, 211 Bryant Space Science Center,
Gainesville, FL 32611-2055*

T. Misawa

Cosmic Radiation Laboratory, RIKEN, 2-1 Hirosawa, Wako, Saitama 351-0198 Japan

D. Tytler

*Center for Astrophysics and Space Sciences, University of California San Diego, La
Jolla, CA 92093-0424, USA*

Abstract

The current paradigm for the AGN phenomenon is a central engine that consists of an inflow of material accreting in the form of a disk onto a super-massive black hole. Observations in the UV and optical find high velocity ionized material outflowing from the black hole. We present results from *Suzaku* and *XMM-Newton* observations of a sample of intrinsic NAL quasars with high velocity outflows. Our derived values of the intrinsic column densities of the X-ray absorbers are consistent with an outflow scenario in which NAL quasars are viewed at smaller inclination angles than BAL quasars. We find that the distributions of α_{OX} and $\Delta\alpha_{\text{OX}}$ of the NAL quasars of our sample differ significantly from those of BAL quasars and SDSS radio-quiet

quasars. The NAL quasars are not significantly absorbed in the X-ray band and the positive values of $\Delta\alpha_{\text{OX}}$ suggest absorption in the UV band. The positive values of $\Delta\alpha_{\text{OX}}$ of the intrinsic NAL quasars can be explained in a geometric scenario where our lines of sight towards the compact X-ray hot coronae of NAL quasars do not traverse the absorbing wind whereas lines of sight towards their UV emitting accretion disks do intercept the outflowing absorbers.

Key words: Techniques:spectroscopic, quasars:general, Galaxies:active

1. Introduction

Optical and UV absorption lines in quasars are commonly classified by their widths into “broad” (BALs; $\text{FWHM} > 2,000 \text{ km s}^{-1}$), “narrow” (NALs; $\text{FWHM} \lesssim 500 \text{ km s}^{-1}$), and mini-BALs with absorption line widths ranging between those of BALs and NALs. These class definitions are considered somewhat arbitrary. The definition of NALs for example was chosen such that the the C IV doublet can be resolved. Several models of quasar structure indicate that the widths of intrinsic absorption lines may depend on the angle between our line of sight and that of the outflowing absorbing stream, and on the velocity gradient in the outflowing stream.

UV spectroscopic observations have revealed highly blueshifted narrow and broad intrinsic absorption lines in quasars implying outflow velocities of up to $\sim 60,000 \text{ km s}^{-1}$ (e.g., [Jannuzi et al. 1996](#); [Hamann et al. 1997](#); [Narayanan et al. 2004](#)). Intrinsic NALs are common in Type I AGN, occurring in $\sim 50\%$ of of optically selected quasars ([Misawa et al. 2007](#)). They may be present in all AGN but only detected in those cases where our line of sight intersects the outflowing absorbing stream. Most of our current understanding of the physical and kinematic structure of NALs and BALs stems from studies of the velocity profiles of absorption lines that appear blueward of resonance UV emission lines. Little is presently known about the absorbing and kinematic properties of these absorption line systems in the X-ray band.

In section §2 we describe the NAL Quasar sample selection, and in §3 the observations, data analysis and results of the sample. Finally in section §4 we conclude by summarizing the results of our observations of NAL quasars.

Throughout this paper we adopt a Λ -dominated cosmology with $H_0 = 70 \text{ km s}^{-1} \text{ Mpc}^{-1}$, $\Omega_\Lambda = 0.7$, and $\Omega_M = 0.3$.

2. NAL Quasar Sample Selection

Our initial NAL quasar sample consisted of $z=2-4$ quasars observed with either the Keck telescope at high spectral resolution for the original purpose of studying intergalactic deuterium lines or quasars obtained from the VLT/UVES archive. The VLT/UVES observations were taken at high spectral resolution ($R \sim 40,000$) for various scientific purposes. From this sample we identified intrinsic NALs by the partial coverage signature of their C IV, N V and S IV absorption doublets (Misawa et al. 2007). The X-ray sample used in this paper consists of 12 $z = 2.2-3.1$ quasars from the initial optical sample that contained intrinsic NALs. The X-ray NAL sample was selected from the initial NAL sample by choosing sources bright enough in the UV resulting in at least 100 counts in the *Suzaku* and/or *XMM-Newton* observations (see Table 1). We have also included in our analysis the 4 NAL quasars from the exploratory survey of Misawa et al. (2008). The X-ray sample does not contain any BAL quasars. Thus our sample consists of secure intrinsic NALs at high ejection velocities, ($63,000 \text{ km/s} \gtrsim v_{\text{ej}} \gtrsim 6,400 \text{ km/s}$). More importantly, the sample is unbiased, selected without regard to quasar properties. Thus it is representative of intrinsic NALs and lends itself to drawing general conclusions about the properties of the absorbers. We note a possible luminosity bias in the X-ray selected sample since we selected the brightest objects from the initial NAL quasar sample to obtain moderate S/N ratio X-ray spectra.

3. X-ray Observations of NAL Quasar Sample

A log of the observations that includes object, observation dates, observatory, observed count rates, total exposure times, and observational identification numbers is presented in Table 1.

In Table 2 we list the redshift, luminosity distance, Galactic column density, flux density at 2500\AA , outflow velocity and the total rest-frame equivalent width (W_{rest}) of the C IV absorption line.

Eleven NAL quasars were observed with *Suzaku* and three with *XMM-Newton*. The *Suzaku* data were collected with the two front-illuminated (FI) CCDs XIS 0, 3 and one back illuminated CCD XIS 1. The *XMM-Newton* data were collected with the EPIC pn and MOS instruments. We used standard *Suzaku* and *XMM-Newton* processing pipeline to reduce the X-ray data.

Object	Observation Date	Observatory	Observation ID	Effective Exposure Time ^a (ks)	N_{sc} ^b
Q0109–3518	2008 May 20	<i>Suzaku</i>	703037010	21.11	332 ± 18
Q0122–380	2008 May 29	<i>Suzaku</i>	703035010	19.14	217 ± 15
Q0329–255	2008 June 16	<i>Suzaku</i>	703038010	21.0	784 ± 28
Q0450–1310	2008 March 10	<i>Suzaku</i>	702062010	7.5	106 ± 10
Q0450–1310	2007 August 10	<i>XMM-Newton</i>	0503350301	5.88	242 ± 16
Q0551–3637	2008 May 14	<i>Suzaku</i>	703036020	8.5	127 ± 11
Q0940–1050	2008 May 5	<i>Suzaku</i>	703040010	18.8	289 ± 52
Q1009+2956	2007 October 31	<i>XMM-Newton</i>	0503350201	5.69	487 ± 22
Q1017+1055	2007 November 27	<i>Suzaku</i>	702064010	8.13	131 ± 12
Q1158–1843	2008 June 19	<i>Suzaku</i>	703039010	7.5	307 ± 41
Q1334–0033	2007 July 14	<i>Suzaku</i>	702067010	12.11	231 ± 15
Q1548+0917	2008 Feb 02	<i>Suzaku</i>	702068010	30.48	612 ± 25
Q1946+7658	2007 July 13	<i>Suzaku</i>	702060010	11.66	398 ± 20
Q1946+7658	2007 July 11	<i>XMM-Newton</i>	0503350101	2.96	200 ± 14

Table 1: Log of Observations of our *Suzaku* and *XMM-Newton* NAL Quasar Sample. ^aEffective exposure time is the time remaining after the application of good time-interval (GTI) tables to remove portions of the observation that were severely contaminated by background. ^b Background-subtracted source counts including events with energies within the 0.2–10 keV band. The source counts and effective exposure times for the *Suzaku* and *XMM-Newton* observations refer to those obtained with the combined XIS units and EPIC PN instrument, respectively.

The X-ray spectra were fitted simultaneously with two models employing XSPEC version 12 (Arnaud 1996). Specifically, the spectral models used in our analysis are the following: (a) A simple power-law, and (b) a simple power-law with intrinsic absorption. All models contain absorption due to our Galaxy.

In Figure 1 (left panels) we show the XIS spectra of three quasars of our sample (first three in Table 1) fit with a model consisting of a power law modified by intrinsic absorption (model b) together with χ^2 residuals of the fits. The right panels of Figure 1 show 68%, 90% and 99% χ^2 confidence contours of N_H versus the photon index, Γ . We find that for all NAL quasars of our sample the χ^2 confidence contours imply no significant intrinsic absorption with the possible exceptions for quasars Q0109-3518 and Q1158-1843 where there is a marginal detection of an intrinsic column density of $N_H \sim$ a few times 10^{22} cm⁻².

In Figure 2 we show the distribution of values of α_{ox} of NAL quasars without correction for intrinsic UV absorption, where, α_{ox} is the optical-to-X-ray slope $\alpha_{ox} = 0.384 \log(f_{2keV}/f_{2500 \text{ \AA}})$ (Tananbaum et al. 1979). Twelve quasars

Quasar	z	D_L^a Gpc	$N_{\text{H}}^{\text{Gal}}$ 10^{20} cm^{-2}	$f_{2 \text{ keV}}^b$ erg s $^{-1} \text{ cm}^{-2} \text{ keV}^{-1}$	$f_{2500\text{\AA}}^c$ mJy	v_{shift}^d km s $^{-1}$	Rest EW Å
Q0109–3518	2.405	20.0	1.93	1.2×10^{-13}	0.261	–62,990	0.064
Q0122–380	2.2	18.0	1.77	4.3×10^{-14}	0.171	–40,613	0.025
Q0329–385	2.423	20.2	1.60	1.1×10^{-13}	0.154	–58,879	
Q0450–1310	2.300	19.0	6.44	3.2×10^{-14}	0.185	–6,369	0.17
Q0551–3637	2.318	19.1	3.15	5.2×10^{-13}	0.165	–51,179	0.3
Q0940–1050	3.080	27.1	4.17	8.5×10^{-14}	0.203	–18,576	0.14
Q1009+2956	2.644	22.5	2.40	1.5×10^{-13}	0.277	–33,879	0.1
Q1017+1055	3.156	27.9	3.66	1.4×10^{-13}	0.083	–47,660	4.92
Q1158–1843	2.448	20.5	3.80	3.0×10^{-13}	0.167	–61,545	0.086
Q1334–0033	2.801	24.1	2.02	3.9×10^{-13}	0.122	–51,040	0.36
Q1548+0917	2.749	23.6	3.43	6.2×10^{-14}	0.057	–36,296	0.32
Q1946+7658	3.051	26.8	7.58	1.4×10^{-13}	0.197	–11,940	0.1

Table 2: The NAL Quasar Sample. ^a The luminosity distance, computed based on the cosmological parameters given at the end of § 1 of the text. ^b Flux density at 2 keV in the quasar rest-frame. Flux densities are derived from the *Suzaku* observations listed in Table 1 with the exception of Q1009+2956 where we use the *XMM-Newton* observation of this object. ^c Flux density per unit frequency at 2500 Å in the quasar rest-frame, derived from the V- or R-band flux (assuming $f_\nu \propto \nu^{-0.44}$) and corrected for Galactic extinction but not intrinsic extinction. ^d Velocity offset of a NAL relative to the redshift of the quasar. A negative value denotes a blueshift.

in this sample are from this study and four are from the [Misawa et al. \(2008\)](#) study. The dashed line shows the distribution of type 1 radio-quiet quasars with l_{2500} values similar to those of our sample (see Table 5 of [Steffen et al. 2006](#)). We notice a significant shift of the α_{ox} distribution of NAL quasars with respect to the optical-selected type 1 SDSS quasars. One possible interpretation of this shift is that on average NAL quasars may be more UV absorbed than type 1 SDSS quasars.

Since α_{ox} is known to correlate with UV luminosity (e.g., [Avni-Tananbaum 1986](#)) we also calculate the parameter $\Delta\alpha_{\text{ox}} = \alpha_{\text{ox}} - \alpha_{\text{ox}}(\ell_{2500\text{\AA}}^\circ)$, where $\alpha_{\text{ox}}(\ell_{2500\text{\AA}}^\circ)$ is the expected α_{ox} for the monochromatic luminosity at 2500 Å (Eq. 6 of [Strateva et al. 2005](#)). $\Delta\alpha_{\text{ox}}$ is a proxy of X-ray weakness corrected for the dependence of α_{ox} on UV luminosity.

In Figure 3 we show the distribution of $\Delta\alpha_{\text{ox}}$ for our current NAL sample, the Steffen et al. 2006 SDSS quasar sample, the [Giustini et al. \(2008\)](#) BAL quasar sample and the [Gallagher et al. \(2006\)](#) LBQS BAL quasar sample. Interestingly our preliminary results hint towards positive values of $\Delta\alpha_{\text{ox}}$ for

NAL quasars.

The positive values of $\Delta\alpha_{\text{OX}}$ of the intrinsic NAL quasars can be explained in a geometric scenario where NAL quasars are viewed at low inclination angles. A possible geometric configuration that can explain this is shown in Figure 4. In this scenario, lines of sight towards the compact X-ray hot coronae of NAL quasars do not traverse the absorbing wind whereas lines of sight towards their UV emitting accretion disks do intercept the outflowing absorbers. Objects that are viewed along lines-of-sight that transverse a substantial portion of the outflowing wind will appear to be Compton thick.

In Figure 5 we show the total rest-frame CIV equivalent width, W_{rest} (top panel), and the maximum NAL velocities of intrinsic CIV NALs of quasars (bottom panel) in our sample (filled circles) and the [Misawa et al. \(2008\)](#) sample (open circles) plotted against α_{ox} (evaluated without corrections for intrinsic absorption). W_{rest} vs. α_{ox} in intrinsic NAL quasars appears to follow the trend of W_{rest} vs. α_{ox} found by [Brandt \(2000\)](#) in low-redshift quasars. It is interesting to point out that the only object from our sample that does not appear to follow this trend is Q1017+1055 that contains both a NAL and a mini-BAL. We finally note that the maximum outflow velocities of the UV absorbers of intrinsic NAL quasars do not appear to be correlated with their X-ray weakness in contrast to what has been reported for BAL quasars (i.e., [Gallagher et al. 2006](#)).

4. CONCLUSIONS

Our results are summarized as follows:

(a) The intrinsic column densities of the X-ray absorbers in our sample of NAL quasars are constrained to be less than a few $\times 10^{22} \text{ cm}^{-2}$. These values of N_{H} are consistent with an outflow scenario in which NAL quasars are viewed at smaller inclination angles than BAL quasars.

(b) The distributions of α_{OX} and $\Delta\alpha_{\text{OX}}$ of the NAL quasars of our sample differ from those of type 1 SDSS radio-quiet quasars and BAL quasars (Figures 2 and 3). The NAL quasars are not significantly absorbed in the X-ray band and the positive values of $\Delta\alpha_{\text{OX}}$ suggest absorption in the UV band.

(c) The positive values of $\Delta\alpha_{\text{OX}}$ of the intrinsic NAL quasars can be explained in a geometric scenario where NAL quasars are viewed at low inclination angles (Figure 4). In this scenario, lines of sight towards a compact X-ray hot coronae of NAL quasars do not traverse the absorbing wind

whereas lines of sight towards their UV emitting accretion disks do intercept the outflowing absorbers.

(d) We find that the maximum outflow velocities of the UV absorbers of NAL quasars are not correlated with their X-ray weakness in contrast to what has been reported for BAL quasars (i.e., [Gallagher et al. 2006](#)).

We acknowledge financial support from NASA grants NNX09AB89G and NNX08AZ67G. ME, JC, and RG acknowledge support from NSF grant AST-0807993.

References

- Arnaud, K. A. 1996, ASP Conf. Ser. 101: Astronomical Data Analysis Software and Systems V, 5, 17
Avni & Tananbaum 1986, ApJ, 305, 83
Brandt et al. 2000, ApJ, 528, 637
Gallagher et al. 2006, ApJ, 644, 709
Giustini et al. 2008, A&A, 491, 425
Misawa et al. 2007, ApJS, 171, 1
Misawa et al. 2008, ApJ, 677, 863
Jannuzi, et al. 1996, ApJ, 470, L11
Hamann et al. 1997, ApJ, 478, 87
Narayanan, et al. 2004, ApJ, 601, 715
Steffen et al. 2006, AJ, 131, 2826
Strateva, et al. 2005, AJ, 130, 387
Tananbaum, et al. 1979, ApJ, 234, L9

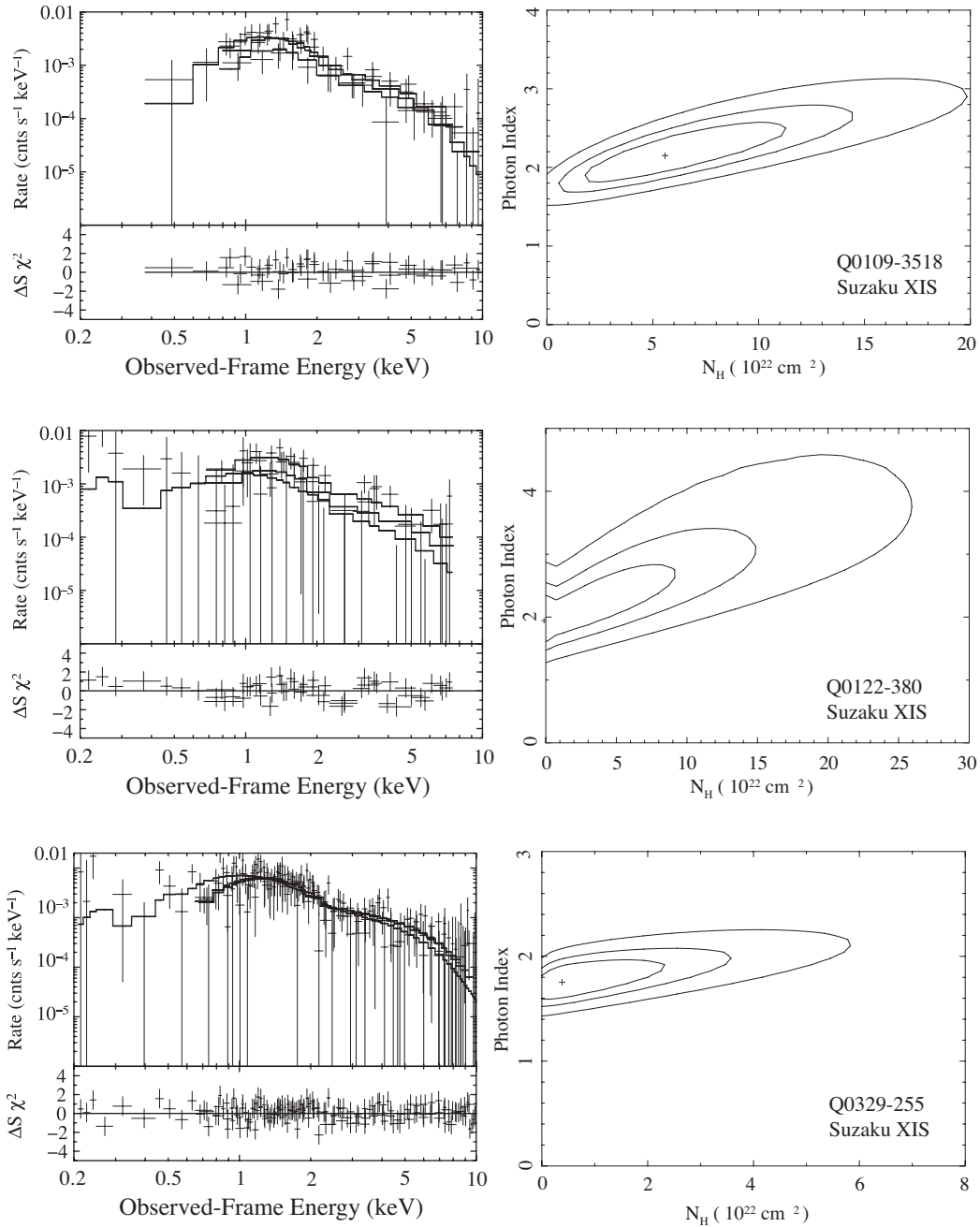


Figure 1: In the left panels we present the XIS spectra of three quasars of our sample fit with a model consisting of a power-law modified by intrinsic absorption (model b) together with χ^2 residuals of the fits. The right panels show the 68%, 90% and 99% χ^2 confidence contours of the intrinsic column density, N_H , versus the photon index, Γ .

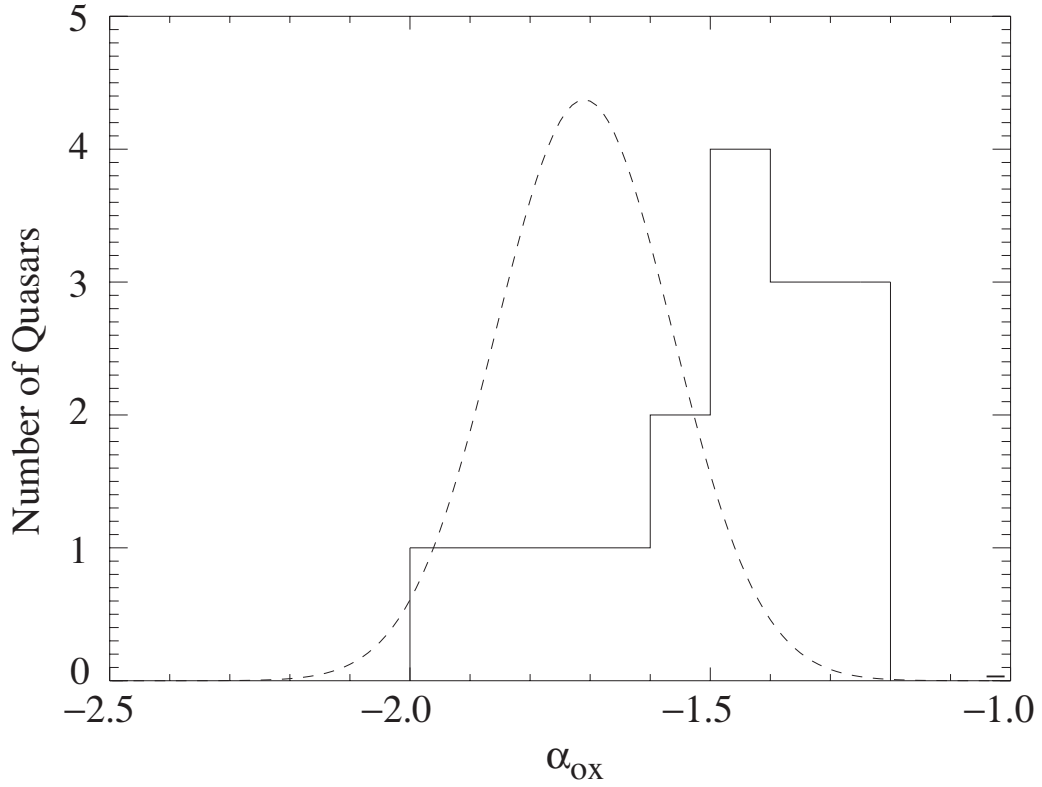


Figure 2: The distribution of values of α_{ox} of NAL quasars without correction for intrinsic UV absorption. Twelve quasars in this sample are from this study and four are from the [Misawa et al. \(2008\)](#) study. The dashed line shows the distribution of type 1 SDSS radio-quiet quasars with l_{2500} values similar to those of our sample ([Steffen et al. 2006](#)). A significant shift of the α_{ox} distribution of NAL quasars with respect to the type 1 SDSS radio-quiet quasars may indicate that on average NAL quasars are more UV absorbed than the SDSS quasars.

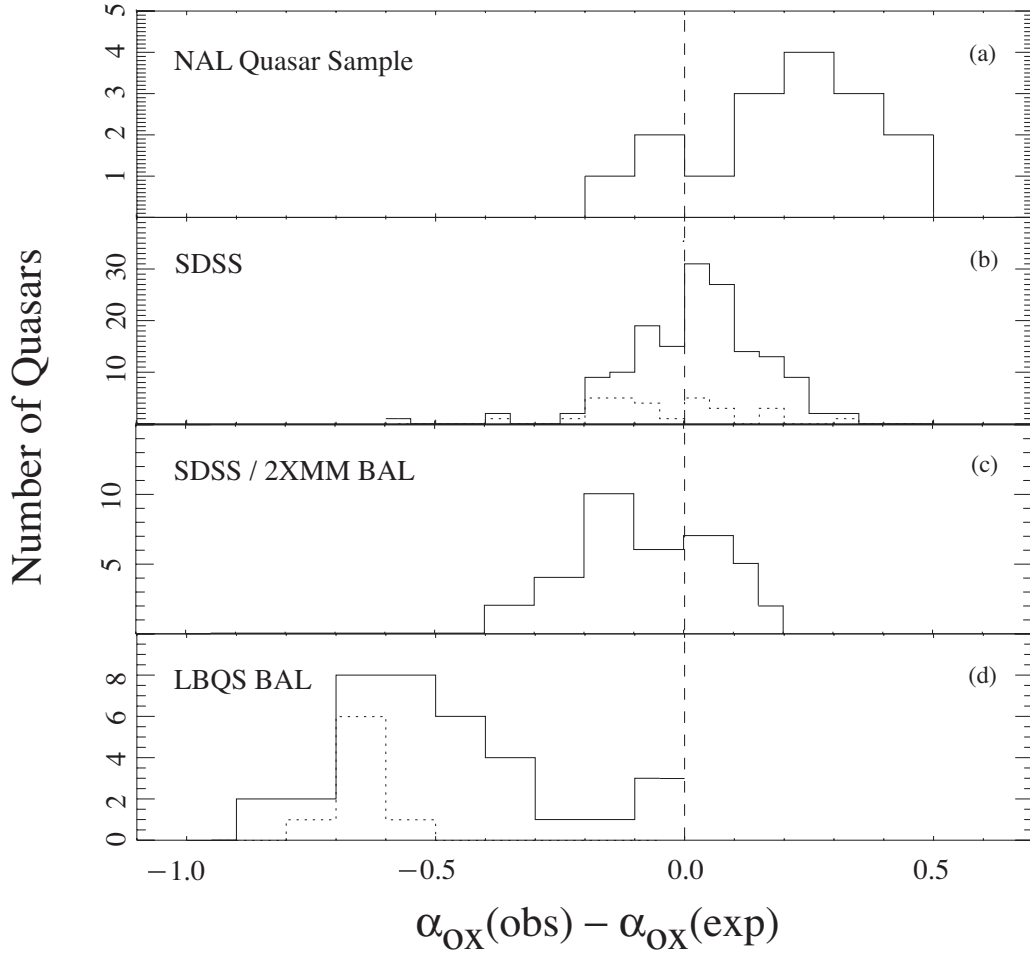


Figure 3: Distribution of $\Delta\alpha_{\text{ox}}$, the difference between the observed value of α_{ox} and the value predicted for that monochromatic UV luminosity by the correlation of [Steffen et al. \(2006\)](#). Negative values of $\Delta\alpha_{\text{ox}}$ indicate a steeper slope than expected. Histograms drawn as dotted lines indicate upper limits. (a): The distribution of $\Delta\alpha_{\text{ox}}$ among quasars in our sample and the [Misawa et al. \(2008\)](#) (without corrections for intrinsic absorption). (b): The distribution of $\Delta\alpha_{\text{ox}}$ among SDSS quasars from [Steffen et al. \(2006\)](#). (c): The distribution of $\Delta\alpha_{\text{ox}}$ among the [Giustini et al. \(2008\)](#) BAL quasar sample. (d): The distribution of $\Delta\alpha_{\text{ox}}$ among BAL quasars from the LBQS (from [Gallagher et al. 2006](#)).

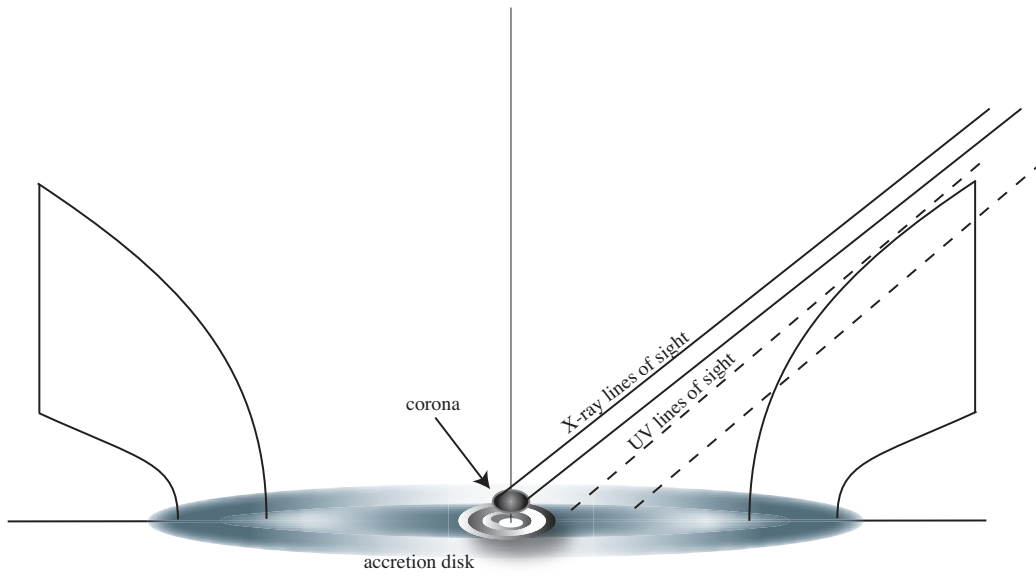


Figure 4: Schematic diagram of a proposed geometry for the accretion disk and associated outflow in quasars. For large inclination angles X-ray emission from the near side of the accretion disk and the central continuum source is blocked by the Compton thick absorbing wind. X-ray lines of sights originating from the corona are indicated with solid lines and UV lines of sight originating from the accretion disk are indicated with dashed lines. Scattered and fluorescent emission from the far side of the accretion disk and outflow may reach the observer. Light rays that originate near the black hole will be slightly bent due to GR effects.

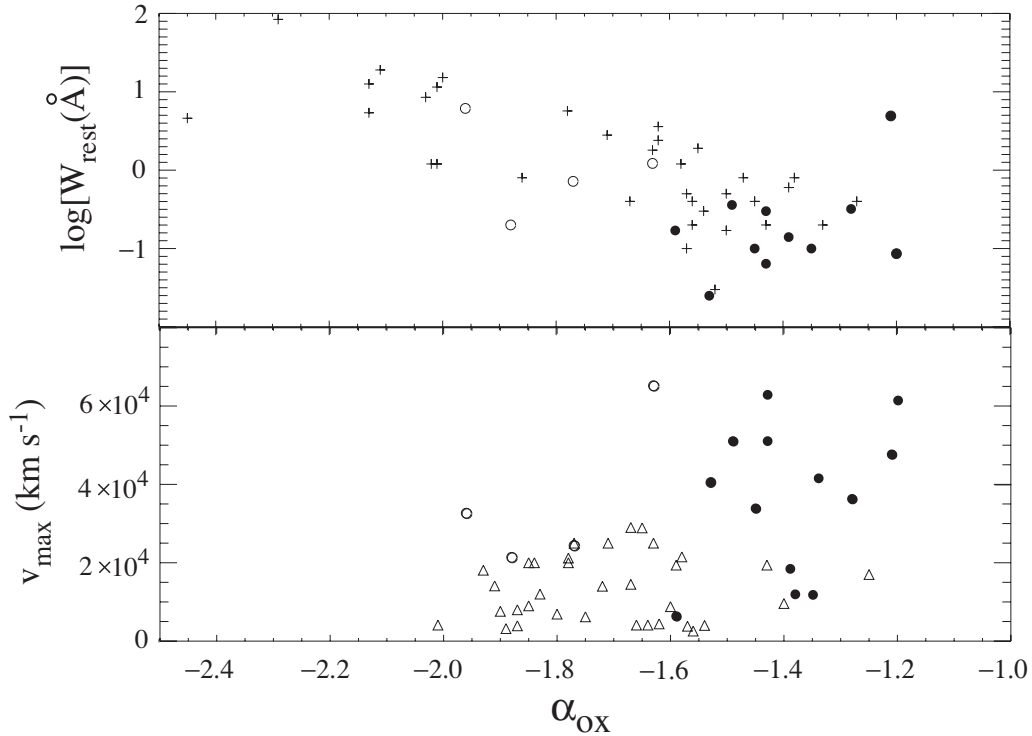


Figure 5: Properties of intrinsic CIV NALs of quasars in our sample (filled circles) and the [Misawa et al. \(2008\)](#) sample (open circles) plotted against α_{OX} (evaluated without corrections for intrinsic absorption). Top Panel: Variation of rest frame equivalent width with α_{OX} . Their rest frame equivalent width is the sum of equivalent widths of all intrinsic NALs in the same quasar. The crosses represent the associated CIV NALs measured in low-redshift quasars by [Brandt \(2000\)](#). Bottom Panel: Variation of the maximum NAL velocity with α_{OX} . The triangles are from the [Giustini et al. \(2008\)](#) BAL quasar sample.